

Shape of the Galactic Orbits in Clusters

Amelia C. Ramírez & Ronaldo E. de Souza

Astronomy Department, University of São Paulo, C.Postal 9638, SP 01065-970, Brazil

e-mail aramirez@kbrita.iagusp.usp.br and ronaldo@kbrita.iagusp.usp.br

ftp: cardeal.iagusp.usp.br anonymous /pub/astro/aramirez

ABSTRACT

A kinematical analysis applied to a sample of galaxy clusters indicates that the differences between the velocity distribution of elliptical and spiral galaxies are associated with the shape of their orbit families. The orbital anisotropies present on each morphological population could be measured with the use of a parameter which is the ratio of the radial and tangential velocity dispersions, and can be recovered through the observed line-of-sight velocity distribution. When a Gaussian velocity distribution is assumed, having different dispersions along the radial and tangential directions, we conclude that the orbits of elliptical galaxies in clusters are close to radial, while spirals have more circular shaped or isotropic orbits. Lenticulars galaxies shares an intermediate orbital parameter, between spirals and ellipticals.

Subject headings: clusters: orbits, morphology — galaxies: kinematic

1. Introduction

As several works have suggested late type galaxies in clusters present a different kinematical behavior compared to early type objects. The cluster velocity dispersion calculated using only spiral galaxy members seems to be always higher than the one calculated using only elliptical galaxies, although at a low significance level. Moreover, late type galaxies tend to present broader spatial distribution when compared to the one observed in early type galaxies, which are more concentrated towards the cluster core. According to Dressler (1980a) this effect is due to the correlation between the frequency of morphological types and the local galaxy density of the clusters. However, Whitmore and Gilmore (1991) proposed that this morphological segregation effect depends upon radial distance to the cluster center instead of the local density. Another difference between late and early type galaxies in clusters, even if marginally supported by observations, is the mass segregation reported by Biviano et al. (1992). They investigate the velocity field of nearby clusters and found that galaxies brighter than the third-ranked object, preferentially bright elliptical galaxies, tend to present velocity dispersion lower than average. They proposed that these objects have suffered the effect of a persistent dynamical friction process.

The explanation to the existence of morphological segregation is still a matter of discussion between the *nurture* and *nature* scenarios of galaxy formation (Bower 1995). Most common interpretations are attributed to the possibility that spirals have been accreted by the cluster more recently, after the collapse and violent relaxation of the initial population of galaxies which now constitute the cluster core (Moss and Dickens 1977, Tully & Shaya 1984, Huchra 1985, Dressler & Shectman 1988, Sodr e et al. 1989, Bird et al. 1994, Andreon 1994, Biviano et al. 1997, Colless & Dunn 1996, Fadda et al. 1996, Girardi et al. 1996, Scodreggio et al. 1995, Andreon & Davoust 1997 and Andreon 1996). When a nurture scenario is assumed it can be expected that during the cluster life different kinematical distribution of their members will produce different interactions and probably different response to them. Thus, the stability of the morphological shapes of galaxies, as they plunge towards the central regions, will depend mostly on their orbits. Some objects, with roughly circular orbits, will not have their morphologies seriously affected because

they avoid the cluster center where the probability of occurring an strong interaction will be larger. However, those with more eccentric orbits will cross the densest cluster regions and will experience on average an stronger environmental influence and a higher encounter rate.

In this paper we present a kinematical analysis of spiral and elliptical galaxies in nearby rich clusters, showing evidences that they represent populations with different families of orbits. Our results impose a further restriction on plausible models of cluster of galaxies formation, where each morphological class must reproduce the corresponding velocity field anisotropy.

In section 2 is presented a discussion of the distribution function we used to analyze the line-of-sight velocities as a function of the adopted anisotropy parameter. In section 3 we define moment statistics over the velocity distribution. In section 4, we use the average deviation of the line-of-sight velocity — the average of the absolute value of the deviation from the mean normalized to the velocity dispersion of the cluster — to trace the orbit distributions of the elliptical and spiral galaxies of a sample of nearby galaxy clusters. In section 5 the velocity dispersion profiles are used to reinforce that our conclusions are in agreement with the best fits to observed clusters made by other authors. In the section 6 we discussed some implications of elliptical galaxies in clusters having more eccentrics orbits. Finally section 7 summarizes our main conclusions.

2. Distribution of velocities on a isotropic Gaussian field

Theoretical models of rich cluster formation predict virialized systems with Maxwellian or nearly Maxwellian velocity distributions, resulting therefore in distributions for the line-of-sight velocities closely described by a Gaussian (Saslaw 1990, Ueda et al. 1993). If clusters are formed by mergers of sub-clumps units, computer simulations suggest that tidal interactions may quickly drive the total gravitational potential toward isothermality. On the other hand, clusters with an isothermal dark matter halo should be single peaked in number density having spherical or elliptical symmetric shapes, with no correlation between the position and velocity of member galaxies, having therefore velocity dispersion independent of the radial position (Roettinger et al. 1993, Katz &

White, 1993).

The above mentioned models leads to the simplest description of clusters structures. However many clusters, having in some cases a large number of measured velocities, present a non-Gaussian projected velocity distribution (Zabludoff et al. 1993). These deviations may imply in anisotropic galaxy orbits and/or mixing of two or more sub-population of galaxies (Merritt 1988, Bird 1994, Merritt & Gebhardt, 1995). In this context, the overall distribution could be non Gaussian even in the presence of different populations, represented by early and late type galaxy members, having individually a Gaussian distribution. Furthermore, different shape of the orbits could produce an additional deviation from gaussianity. To test these hypothesis, we studied the velocity distribution of each morphological population to verify if they show signs of non-isotropic distributions.

To study the velocity distribution of a population, being less restrictive as possible, Merritt & Gebhardt (1995) used directly the observed data, fitting their velocity distribution profiles with few or any parameter at all in order to obtain a unique solution. In our case however, since we are interested in the study of the orbital anisotropy we rather prefer to use a parameterized statistics related to a Gaussian distribution. Even if that assumption may not accurately represent the true velocity distribution due to its simplicity, it can be useful as a first approximation to understand the effects of the anisotropy in the overall cluster structure.

We assume that for a given morphological class the velocity distribution function is Gaussian, having however different dispersions along the radial (σ_R) and transversal directions (σ_\perp). The behavior of the velocity distribution of this system can therefore be described by the anisotropy parameter $\eta = \sigma_R/\sigma_\perp$. A large value of η for a given population means that its members are crossing the cluster with an almost radial orbit, and therefore are more sensitive to suffer gravitational encounters with objects in the dense central regions. On the contrary, objects with lower anisotropy parameter tend to have a more circular orbit with small penetration in the dense core region. Therefore, on a given morphological class the anisotropy parameter should allow us to connect the efficiency of the environment perturbations with the related kinematical orbital behavior.

At the present it is not yet well understood the influence of the projection effects, due to foreground

and background galaxies, and the cluster substructure on the studies of cluster dynamics. However we could expect that their presence should introduce some deviation from the simplest cluster models scenario. We will consider the dynamical behavior of a cluster without taking into account these effects, but we return to this point late in the section 4.

For a radially symmetric cluster the velocity distribution along the line-of-sight can be derived from the assumed spatial velocity distribution. Then, for a given morphological class we will further assume that the anisotropy η parameter have a fixed value, and consequently the probability of finding an object at a given position and velocity is determined by the expression,

$$dN(R, \theta, \phi; v_R, v_\theta, v_\phi) = n(R)R^2 \sin \theta dR d\theta d\phi \times \\ \frac{1}{(2\pi)^{3/2} \sigma_R \sigma_\perp^2} e^{-\frac{v_R^2}{2\sigma_R^2} - \frac{(v_\phi^2 + v_\theta^2)}{2\sigma_\perp^2}} dv_R dv_\phi dv_\theta$$

where $n(R)$ is the density profile. Since the velocity distribution does not depend on R , and the density is spherically symmetric, we can easily integrate the radial contribution and also the terms related to the spatial azimuthal coordinate to obtain,

$$dN(\theta; v_R, v_\theta, v_\phi) = \frac{N}{2} \sin \theta d\theta \frac{1}{(2\pi)^{3/2} \sigma_R \sigma_\perp^2} \times \\ e^{-\frac{v_R^2}{2\sigma_R^2} - \frac{(v_\phi^2 + v_\theta^2)}{2\sigma_\perp^2}} dv_R dv_\phi dv_\theta$$

where N represents the total number of objects in the system.

In order to obtain the observed velocity distribution a better choice is to use the cylindrical coordinates v_r, v_z, v_ϕ , where v_z is directed along the line-of-sight. The transversal component to the line of sight, v_ϕ , is independent of the angle θ , and can be integrated to obtain,

$$dN(\theta; v_r, v_z) = \frac{N}{2} \frac{1}{2\pi \sigma_R \sigma_\perp} e^{-\frac{v_r^2}{2\sigma_R^2} - \frac{v_z^2}{2\sigma_\perp^2}} \sin \theta d\theta dv_r dv_z$$

This equation can be further integrated using the transformations $v_R = v_r \sin \theta + v_z \cos \theta$, and $v_\theta = v_r \cos \theta - v_z \sin \theta$, and changing variables to $p = v_r/\sigma_R$

and $q = v_z/\sigma_R$. Using these relations we can express the observed velocity distribution along the line-of-sight in the form,

$$\frac{dN(q)}{dq} = \frac{N}{2} \int_0^\pi \sin \theta \int_{-\infty}^{\infty} \frac{\eta}{2\pi} \times e^{-\frac{(p \sin \theta + q \cos \theta)^2}{2} - \frac{\eta^2 (p \cos \theta - q \sin \theta)^2}{2}} dp d\theta$$

After some manipulation to complete the square term entering in the internal expression, the integral related to the velocity term (p) can be solved exactly. Since the mean expected velocity dispersion can be expressed in the form $\sigma = \sqrt{(\sigma_R^2 + 2\sigma_\perp^2)/3}$, we may use it to define a more interesting reduced variable $u = v_z/\sigma$. Introducing the symbol $\omega = \cos \theta$, we finally obtain the line-of-sight velocity density distribution in the form,

$$F(u; \eta) = \frac{1}{(2\pi)^{1/2}} \int_0^1 \frac{1}{\Theta(\omega, \eta)} e^{-\frac{u^2}{2\Theta(\omega, \eta)^2}} d\omega \quad (1)$$

where the term $\Theta(\omega, \eta) = \sqrt{\frac{3(1-\omega^2+\eta^2\omega^2)}{2+\eta^2}}$ represents a correction of the velocity dispersion due to the presence of the anisotropic field. This equation corresponds to the line-of-sight velocity distribution in a Gaussian velocity field with anisotropy and can only be solved numerically. In Figure 1 we present this distribution for some representative values of the anisotropic parameter. In particular, for $\eta = 1$ we retrieve the expected Gaussian shape for an isotropic velocity field. We remark that, even if the radial and transversal distributions are assumed to be Gaussian, the observed distribution along the line-of-sight is not Gaussian when the anisotropy parameter is different of one.

2.1. Average deviation, kurtosis and peak value of $F(u; \eta)$

Although in the general case the line-of-sight velocity density distribution can be estimated only by numerical methods, it is interesting to note that the expressions for the moments can be solved exactly. The distribution $F(u; \eta)$ is symmetric by construction, resulting that the first centered moment is obviously zero. The second moment corresponds to the variance of the distribution and can be estimated by the expression,

$$\sigma_u^2 = \int_{-\infty}^{\infty} u^2 \frac{1}{(2\pi)^{1/2}} \int_0^1 \frac{1}{\Theta(\omega, \eta)} e^{-\frac{u^2}{2\Theta(\omega, \eta)^2}} d\omega du \quad (2)$$

inverting the order of integration we can easily show that the function Θ is eliminated before doing the second integration, resulting that the velocity dispersion remains independent of the anisotropic parameter. Therefore, we may expect that two populations responding to the same potential can present different orbital shapes, but their velocity dispersions remains constant.

The central peak value of the distribution $F(0; \eta)$ may also be easily integrated resulting in the expression,

$$F(0; \eta) = \sqrt{\frac{2 + \eta^2}{6\pi(\eta^2 - 1)}} \ln(\sqrt{\eta^2 - 1} + \eta) \quad \eta^2 > 1 \quad (3)$$

$$F(0; \eta) = \sqrt{\frac{2 + \eta^2}{6\pi(1 - \eta^2)}} \sin^{-1}(\sqrt{1 - \eta^2}) \quad \eta^2 < 1 \quad (4)$$

An interesting feature is that the central value of this distribution is bounded to a limiting value $\frac{1}{\sqrt{6\pi}} \ln(2\eta)$ for $\eta \gg 1$, while for $\eta \ll 1$ the central density approaches to the limit $\sqrt{\pi/12} \simeq 0.51$. For $\eta = 1$ the central value tends to $1/\sqrt{2\pi}$, characteristic of the Gaussian distribution.

We may also obtain the fourth order moment and consequently the kurtosis,

$$K = \frac{12}{5} \left(\frac{\eta^2 - 1}{\eta^2 + 2} \right)^2 \quad (5)$$

For highly radial orbits ($\eta \gg 1$) the kurtosis approaches the limit $K \simeq 2.4$, while for circular orbits ($\eta \ll 1$) $K \simeq 0.6$. Moreover the minimum kurtosis ($K = 0$) is attained for $\eta = 1$ when the distribution is normal.

A disadvantage of using the kurtosis, or the $F(0; \eta)$, as indicative for the anisotropy parameter, is their large sampling error. To overcome this difficulty we propose the use of the average or mean deviation (Kendall, Stuart and Ord, 1987) of the line-of-sight velocity normalized to the velocity dispersion

($|u| = \langle \frac{|v-\bar{v}|}{\sigma} \rangle$). The predicted value of this statistical parameter can be estimated by the expressions,

$$|u| = \sqrt{\frac{6}{\pi(\eta^2 + 2)}} \left(\frac{\eta}{2} + \frac{1}{2} \frac{1}{\sqrt{1-\eta^2}} \sin^{-1}(\sqrt{1-\eta^2}) \right)$$

$$\eta < 1$$

$$|u| = \sqrt{\frac{6}{\pi(\eta^2 + 2)}} \left(\frac{\eta}{2} + \frac{1}{2} \frac{1}{\sqrt{\eta^2 - 1}} \ln(\sqrt{\eta^2 - 1} + \eta) \right)$$

$$\eta > 1$$

For purely radial orbits ($\eta \gg 1$) $|u| \rightarrow \sqrt{3/2\pi} \simeq 0.69$, while for circular orbits ($\eta = 0$) $|u| = \sqrt{3\pi}/4 \simeq 0.77$. In the case of $\eta = 1$ we have a Gaussian distribution and we recover the value $|u| = \sqrt{2/\pi} \simeq 0.80$.

In Figure 2 we show these three statistical parameters as a function of η . We observe that they have an extrema at $\eta = 1$, producing an indetermination when we try to derive η from the estimated values of these quantities. In fact, using these parameters we cannot distinguish between a purely circular model ($\eta = 0$) and another one having a radial contribution slightly higher than the isotropic case. The worse indetermination occurs when we use the peak value statistics, since in that case we cannot distinguish between a circular orbit model and another one having $\eta \leq 4$. The kurtosis and the average deviation of the line-of-sight velocity, reduce this indetermination to a region with $\eta \leq 2$. Due to this limitation we will restrict our analysis to a discussion of the kurtosis and the average deviation. However, it is interesting to note that highly radial models can be easily discriminated, using any one of these indicators, since in that case the velocity distribution is highly peaked, as can be seeing also from Figure 1.

3. The sample of galaxy clusters

A sample of nearby rich clusters was selected to test for the presence of systematic differences of orbital parameters among the morphological populations. We have collected material for all clusters with $z < 0.055$ from a catalogue of measured redshifts of Abell clusters compiled by Andernach (1991). This redshift limit was adopted in order to avoid dealing with morphological misclassification. From a total of 1059 clusters only 323 have $z < 0.055$, most of them with less than 10 velocities published in the literature. We selected for our tests only those having at

least 65 objects with measured velocities and morphologically classified as elliptical, spiral or lenticular galaxies, within $2.5 h^{-1}$ Mpc from the cluster center. We have also discarded clusters with obvious substructures, since in those cases the velocity distribution could result from a complex association of several small groups. Half of the clusters with at least 65 members with radial velocities don't fill the morphological requirement which is essential for our purposes. Therefore, we reach a final sample having only 18 clusters that satisfied the velocity, spatial and population requirements.

The association of a galaxy with a given cluster was decided on basis of the following procedure. For each cluster we have estimated the mean heliocentric velocity, and the raw velocity dispersion along the line-of-sight. This was determined taking into account all galaxies within $5.0 h^{-1}$ Mpc of the nominal center of each cluster and considering objects of all morphological classes. The sample of velocity data for each cluster was selected using the HEASARC¹ facilities and completed with the CfA Redshift Catalog (ZCAT/version November/1995, Huchra et al. 1992). The velocities published by Biviano et al. (1996), Colless & Dunn, (1996), and the PGC Catalog (Paturel et al. 1989) were also used. Non-member galaxies were detected by the classical $3\text{-}\sigma$ test (Yahil & Vidal, 1977). Finally, we concentrated our estimatives to an outer radius of $2.5 h^{-1}$ Mpc and selected only elliptical, spiral and lenticular galaxies. At this point, new values of mean velocity and velocity dispersion for the cluster and for each morphological population were obtained. All the mean values and dispersions (location and scale values in the robust statistical notation) were calculated with the bi-weighted estimators, using the ROSTAT² program which contains the versions of statistical routines tested by T. Beers, K. Flynn, and K. Gebhardt for robust estimation of simple statistics and described in Beers et al. (1990). All the errors bars appearing in this paper are at the 68% confidence level, and were obtained via a bootstrap resampling procedure with 1000 iterations.

The morphological classification was extracted from Dressler (1980b), and The Third Reference Catalog of Bright Galaxies (RC3) (de Vaucouleurs et al. 1991).

¹High Energy Astrophysics Science Archive Research Center Online Service, provided by the NASA/Goddard Space Flight Center

²Version obtained from the ST-ECF Astronomical Software Library ftp://ecf.hq.eso.org/pub/swlib

TABLE 1
CLUSTER KINEMATIC PARAMETERS USING THE ELLIPTICAL, SPIRAL AND LENTICULAR GALAXIES

Name	N	r_{200} Mpc	r_h Mpc	v_{BI} km/s	σ_{BI} km/s	K		$ u _{cl}$	$\sigma_{ u }$	References				
All														
A1656	458	1.8	0.9	6969	48	1032	39	0.8	0.22	0.71	0.03	0.59	0.03	zcat; CD95 ^a &B96 ^b
Virgo	402	1.4	1.4	1380	39	785	23	-0.6	0.24	0.76	0.03	0.55	0.02	zcat
A3526	287	1.5	1.2	3436	51	863	34	-0.7	0.29	0.75	0.04	0.60	0.02	zcat; Centaurus
A0194	146	0.7	0.9	5338	33	398	28	1.1	0.41	0.71	0.05	0.64	0.06	zcat
A0548	128	1.5	1.4	12407	77	870	45	-0.9	0.43	0.83	0.05	0.52	0.03	zcat
A1060	98	1.1	0.7	3668	64	631	44	-0.5	0.49	0.74	0.06	0.59	0.04	zcat; Hydra
A2151	93	1.3	1.3	11000	76	735	46	-0.7	0.51	0.80	0.06	0.59	0.04	zcat; Hercules
A1644	89	1.6	1.6	14129	99	934	84	0.3	0.52	0.67	0.06	0.59	0.09	zcat
A0539	83	1.2	0.8	8721	79	715	72	0.2	0.54	0.66	0.07	0.67	0.07	zcat
A463s	79	1.1	1.1	12275	71	624	37	-0.9	0.55	0.83	0.06	0.51	0.04	zcat; DC0428-53
A0496	77	1.1	0.6	9836	71	620	67	0.4	0.56	0.64	0.08	0.66	0.09	zcat
	138			9870	62	728	49	0.0	0.42	0.70	0.05			M92 ^c
A3376	77	1.3	1.1	13909	84	737	72	0.3	0.56	0.70	0.08	0.65	0.07	zcat; DC0559-40
A805s	77	0.7	0.7	4351	48	419	38	0.1	0.56	0.71	0.07	0.57	0.06	zcat; DC1842-63
	114			4513	47	503	44	0.1	0.46	0.66	0.06			M92 ^c
A0119	76	1.5	0.9	13324	97	840	91	0.0	0.56	0.66	0.08	0.68	0.08	F93 ^d
A0754	72	1.4	1.4	16257	96	812	84	-0.1	0.58	0.70	0.08	0.64	0.08	zcat
A1983	72	1.1	1.5	13562	78	660	153	1.5	0.58	0.52	0.07	0.56	0.10	zcat
A1631	68	1.2	1.5	13971	85	696	50	-0.6	0.59	0.79	0.07	0.58	0.04	zcat
Fornax	66	0.6	0.7	1483	41	330	24	-0.6	0.60	0.76	0.07	0.58	0.05	F89 ^e
Spirals														
A1656	189	1.9	1.0	7036	79	1082	66	0.7	0.36	0.73	0.05	0.61	0.04	
Virgo	265	1.4	1.6	1414	51	824	26	-0.8	0.30	0.82	0.03	0.57	0.02	
A3526	155	1.5	1.7	3390	67	838	51	0.6	0.39	0.71	0.05	0.59	0.04	
A0194	76	0.7	1.4	5306	47	410	32	-0.2	0.56	0.78	0.06	0.63	0.11	
A0548	45	1.7	1.4	12407	151	1002	81	-1.1	0.73	0.97	0.09	0.59	0.05	
A1060	36	1.1	1.1	3506	103	611	50	-0.6	0.82	0.72	0.10	0.57	0.08	
A2151	45	1.2	1.1	11265	106	706	64	-0.4	0.73	0.72	0.09	0.65	0.05	
A1644	23	1.7	1.8	13808	211	987	171	-0.1	1.02	0.68	0.13	0.69	0.11	
A0539	41	1.0	1.6	8726	94	597	85	0.1	0.77	0.53	0.08	0.50	0.09	
A463s	18	1.3	1.7	12215	186	754	114	-1.0	1.15	0.95	0.17	0.67	0.10	
A0496	18	1.1	1.2	10055	150	612	102	-0.8	1.15	0.74	0.13	0.63	0.15	
A3376	24	1.3	1.3	13845	164	779	122	-0.1	1.00	0.75	0.13	0.60	0.12	
A805s	39	0.8	1.7	4395	70	434	63	0.0	0.78	0.70	0.11	0.65	0.10	
A0119	15	1.7	1.3	13687	261	959	143	-1.0	1.26	0.94	0.17	0.68	0.10	
A0754	25	1.5	1.6	16347	178	869	156	-0.2	0.98	0.75	0.14	0.71	0.19	
A1983	31	2.1	1.5	13353	220	1194	426	0.3	0.88	0.72	0.23	1.10	0.63	
A1631	16	1.2	1.5	14215	178	676	139	0.0	1.22	0.70	0.14	0.62	0.10	
Fornax	22	0.6	0.8	1548	82	371	52	-0.9	1.04	0.84	0.13	0.56	0.07	

There were 322 objects not classified in the cited references, in these cases one of us (AR) have classified them using the images from the Digitized Sky Survey from the STScI. In all cases, these galaxies are members of clusters having some objects already classified, allowing us to compare our classification scheme with the original published classification. Clusters with radial velocity but with no classification at all, as A85 or DC0107-46 were not included in our analysis because a good morphological classification was not guaranteed. We have adopted a very simple classification scheme dividing objects in ellipticals, dwarf ellipticals, spirals, dwarf spirals, lenticulars, irregulars and unknowns, in the case we couldn't find a suitable class. A random sample of objects was selected for testing the classification procedure, and the comparison of our classification with the RC3 catalog and Dressler (1980b) is within the range of agreement among traditional morphologists, 75% to 80% (Andreon, 1996). As expected we noted that the miss-identification of the morphological class is larger in the case of lenticular galaxies.

A mean synthetic cluster, (MSC), was built by adding the velocity, position and morphology information of all galaxies from the clusters in our sample. The velocities of each object were corrected for the mean velocity of the host cluster and normalized by the corresponding velocity dispersion. Their relative positions inside the cluster were also normalized using a fiducial radius. Hopefully this average synthetic cluster preserves the radial dependence of kinematical properties of the sample, clearing off the effects due to eventually present local substructures.

In Figure 3 we present the space distribution, the average deviation as a function of the normalized radius, and the line-of-sight velocity histograms of all galaxies separated by morphological populations of the MSC cluster. The left panels from top to bottom present the projected position of spirals, lenticulars and ellipticals. As we mention before, the positions were scaled using as fiducial radius the so called virial radius, r_{200} , used by Carlberg et al. (1997) and defined as,

$$r_{200} = \frac{\sqrt{3}\sigma}{10H(z)}$$

where σ is the global velocity dispersion of each cluster and the Hubble constant $H(z)$ in our case was adopted as $H_0=100 \text{ kms}^{-1}\text{Mpc}^{-1}$. This radius, defined as the radius where the mean interior density

is 200 times the critical density of the universe, is expected to contain the bulk of the virialized cluster mass. The middle panels show, the absolute value of all velocities normalized to the corresponding global cluster dispersion as a function of the normalized radius. Using this data we estimated the average deviation ($|u|$) within radial rings having 100 galaxies each (solid lines). The dashed line shows the expected value for the case of isotropic orbits ($|u| \sim 0.8$). The right panels show the histograms of the relative velocities normalized to the corresponding velocity dispersion.

From Figure 3 we conclude that spirals tend to present a broader distribution in space and also in velocities distribution. On the contrary the distribution of ellipticals is more concentrated, in both positions and velocities, reflecting the presence of the morphological segregation inside each individual cluster. Although there is a large spread in the velocity distribution, we observe that the average deviation of ellipticals as a function of radius seems to have values always lower than the expectation value for isotropic orbits indicating more eccentric orbits and showing again a different behavior from spirals. Finally, it is interesting to note that lenticular galaxies show an intermediate behavior between spirals and ellipticals. We can also observe that spirals in the outer region ($r > r_{200}$) tend to present more eccentric orbits, as indicated by the lower values of the average deviation of velocity distribution.

To test the normality of the velocity distributions, shown in the right panels of Figure 3, we have applied the Kolmogorov-Smirnov statistic, and an improved W-test (Yahil and Vidal, 1977). In both cases the probability to reject the hypothesis is of the order of 25%. Therefore, although the significance level is low, we cannot reject that these distributions could be described by a Gaussian distribution.

The individual properties of the clusters are summarized in Table 1, separated by morphological classes. Columns (1) and (2) show the name of the cluster and the number of galaxies within $2.5 h^{-1}\text{Mpc}$. In column (3) we present the r_{200} radius in $h^{-1}\text{Mpc}$ and column (4) shows the harmonic radius, r_h , which gives a estimation of the mean projected separation between galaxies inside each cluster. In columns (5) and (6) we show the mean velocity (v_{BI}) and velocity dispersion (σ_{BI}) in km s^{-1} , together with their errors at the 68% confidence level. Columns (7) and (8) show the kurtosis and the average deviation of the line-of-sight

TABLE 1—*Continued*

Name	N	r_{200} Mpc	r_h Mpc	v_{BI} km/s	σ_{BI} km/s	K		$ u _{cl}$		$\sigma_{ u }$	References		
Lenticulars													
A1656	111	1.9	0.8	6864	106	1120	85	0.4	0.46	0.76	0.05	0.58	0.06
Virgo	81	1.2	1.0	1418	76	680	48	-0.6	0.54	0.65	0.05	0.46	0.05
A3526	85	1.5	1.1	3501	96	878	77	-0.6	0.53	0.72	0.07	0.65	0.04
A0194	35	0.6	0.7	5397	57	330	89	-0.8	0.83	0.53	0.10	0.54	0.13
A0548	52	1.4	1.3	12415	110	784	57	-1.0	0.68	0.75	0.07	0.50	0.03
A1060	49	1.1	0.6	3795	93	642	52	-0.8	0.70	0.79	0.08	0.60	0.05
A2151	36	1.3	1.2	10855	130	768	64	-1.2	0.82	0.89	0.08	0.56	0.07
A1644	47	1.5	1.5	14207	124	840	104	0.5	0.71	0.64	0.08	0.48	0.09
A0539	31	1.6	0.5	8726	167	911	126	-0.9	0.88	0.94	0.15	0.82	0.09
A463s	39	1.0	1.2	12238	96	592	57	-0.5	0.78	0.78	0.09	0.52	0.05
A0496	32	1.3	0.5	9706	132	733	108	-0.1	0.87	0.85	0.14	0.80	0.12
A3376	40	1.4	1.2	13846	128	801	104	0.2	0.77	0.79	0.11	0.71	0.10
A805s	29	0.6	0.6	4351	70	368	39	2.2	0.91	0.69	0.09	0.46	0.06
A0119	36	1.3	1.1	13243	123	729	121	0.5	0.82	0.55	0.08	0.56	0.11
A0754	25	1.2	1.5	16072	140	680	82	-0.9	0.98	0.67	0.11	0.50	0.06
A1983	27	0.7	1.7	13681	83	422	286	1.0	0.94	0.37	0.08	0.35	0.13
A1631	43	1.3	1.4	13941	112	728	71	-0.6	0.75	0.82	0.09	0.60	0.06
Fornax	24	0.6	0.6	1507	68	323	49	-0.2	1.00	0.68	0.10	0.51	0.10
Ellipticals													
A1656	158	1.6	0.8	6958	72	908	63	1.2	0.39	0.61	0.04	0.55	0.05
Virgo	56	1.2	0.8	1172	94	701	78	0.2	0.65	0.61	0.08	0.50	0.06
A3526	47	1.6	0.7	3472	133	902	66	-1.2	0.71	0.86	0.08	0.54	0.04
A0194	35	0.7	0.9	5344	68	398	66	1.5	0.83	0.64	0.11	0.65	0.12
A0548	31	1.5	1.3	12391	154	841	93	-0.7	0.88	0.78	0.08	0.45	0.07
A1060	13	1.0	0.6	3660	175	596	166	0.0	1.36	0.48	0.16	0.49	0.40
A2151	12	0.6	1.6	10522	114	369	53	-1.4	1.41	0.44	0.08	0.47	0.06
A1644	19	1.8	1.9	14252	254	1067	244	-0.3	1.12	0.70	0.18	0.75	0.25
A0539	11	1.0	0.2	8729	194	601	279	0.4	1.48	0.38	0.19	0.56	0.37
A463s	22	1.1	1.0	12495	143	649	209	-1.3	1.04	0.75	0.13	0.32	0.05
A0496	27	0.8	0.2	9818	88	445	126	1.5	0.94	0.43	0.09	0.46	0.09
A3376	13	0.7	0.5	14050	123	417	133	0.4	1.36	0.33	0.05	0.39	0.22
A805s	9	0.9	0.3	4111	186	507	151	-0.4	1.63	0.70	0.19	0.81	0.30
A0119	24	1.5	0.6	13394	180	859	349	-0.1	1.00	0.42	0.14	0.79	0.42
A0754	22	1.5	0.8	16451	195	885	167	-0.2	1.04	0.77	0.16	0.76	0.24
A1983	14	0.9	0.6	13575	145	514	111	-0.9	1.31	0.57	0.12	0.42	0.11
A1631	9	0.9	0.9	13706	181	493	85	-1.4	1.63	0.60	0.13	0.46	0.14
Fornax	20	0.5	0.5	1396	64	277	80	-0.1	1.10	0.49	0.14	0.58	0.60

^aColless and Dunn (1996)^bBiviano et al.(1996)^cMalumuth et al. (1992)^dFabricant et al. (1993)^eFerguson (1989)

velocity, $|u|_{cl}$, with their respective errors at the 68% confidence level. Column (9) shows the dispersion of the cluster average deviation, and finally column (10) shows the velocity references and the other names as the cluster is known. Each selected cluster has four entries in this table, one corresponding to the data of all objects irrespective of their morphological type and one entry only for the spirals, lenticulars and ellipticals.

We have mentioned at the beginning of this section that in some cases a larger number of published velocities are available, but without morphological classification. To estimate the influence of the velocity incompleteness on our mean values, presented in Table 1, we have also estimated the kinematical parameters using all the published velocities for two clusters (second lines in A496 and A805s entries). For these two clusters the total number of galaxies is almost a factor two larger than the number of objects having morphological information. Nevertheless, the differences in the average deviation are well within the error bars, showing that the velocity incompleteness does not affect drastically our results. In section 4 we will return to this point using the data for Virgo and Coma, where we have a larger number of data.

In section 2, we show that the expected value of the average deviation is independent of the expected value of the velocity dispersion. It means that two populations having the same velocity dispersion may present different anisotropies, and consequently different values of the average deviation. Therefore we would expect that the measured velocity dispersion on Table 1 should be independent of the morphological class, if they were subjected to the same gravitational potential and having a common Gaussian velocity distribution with spherical symmetry. However we notice that there are some small, but systematic, differences between the velocity dispersion of each morphological classes. A possible explanation of these differences is discussed in the section 5. However, for our present purposes the existence of this difference poses a conceptual problem since we need to define the average deviation normalized by the velocity dispersion. In the present analysis we have used all the average deviations normalized to the velocity dispersion deduced from the whole cluster population. Actually, we repeat the same analysis but normalizing to the velocity dispersion of each morphological class and it makes no difference in our conclusions, except for an small increase in the errors. The reason, is

that this morphological segregation on the velocities dispersions is small enough to not significantly affect the determination of the average deviation.

4. Average deviation of the line-of-sight velocity

In Figure 4 we show the histograms of the average deviation of the line-of-sight velocity for the 18 clusters presented in Table 1. The upper panel represents the spiral population, the middle panel the lenticulars, and the lower one the ellipticals. In the left set of panels we present the histograms of the central region, around $1.0 h^{-1} \text{ Mpc}$, of each cluster, while in the right panels the whole $2.5 h^{-1} \text{ Mpc}$ region. The open histogram represent the contribution of clusters were there might be some suspicious of low level substructures as detected by Girardi et al. (1996). The vertical dashed lines show the expected value for the extreme cases of radial (R) and circular (C) orbits for our Gaussian model discussed in the previous sections.

Although all histograms present a large intersection region, it remains true that spirals tend to peak around $|\bar{u}| = 0.74 \pm 0.12$ in the $2.5 h^{-1} \text{ Mpc}$ sample and $|\bar{u}| = 0.80 \pm 0.17$ in the $1.0 h^{-1} \text{ Mpc}$ region. These values are close to the prediction of a pure circular ($|u|_{cir} \sim 0.77$), or isotropic ($|u|_{iso} \sim 0.80$) models, although as remarked in section 2 we cannot distinguish between the circular case ($\eta = 0$), the isotropic case ($\eta = 1$), and an slightly radial case having $\eta \sim 2$. On the other hand the elliptical distribution peaks in the region $|\bar{u}| = 0.59 \pm 0.13$ and $|\bar{u}| = 0.59 \pm 0.14$ for $2.5 h^{-1} \text{ Mpc}$ and $1.0 h^{-1} \text{ Mpc}$, respectively, both values close to the prediction of the radial orbit limit ($|u|_{rad} \sim 0.69$). We remark that this limit is the lowest value permitted by the simple Gaussian distribution adopted in the present analysis. We can observe from Figure 4 that several clusters have mean deviations below that limit. This is a limitation of the present model, as will be discussed in section 5.

The difference between the behavior of spirals and ellipticals is persistent in both, central ($1.0 h^{-1} \text{ Mpc}$) region and the whole ($2.5 h^{-1} \text{ Mpc}$) cluster. To further clarify this point and quantify the degree of significance of these differences we have applied some statistical tests to verify (1) if the distributions comes from a normal distribution and (2) that distributions of different morphological class comes from the same parent distribution. To test the normality we used

the modified Kolmogorov-Smirnov statistic, and an improved W-test (Yahil and Vidal, 1977). In Table 2 we present the mean values and the results of these two tests applied to the observed distribution of the average deviation values. Here we have in column (1) the morphological population, in column (2) the characteristic of the sample considering only those clusters *Without substructures* and *All clusters*. In column (3) we have the number of clusters included in the respective sample and in column (4) the outer limiting radius in h^{-1} Mpc. Again, we divided the data into one sample well inside the expected virialized region and a complementary region containing all the cluster members. Column (5) shows the mean of the average deviation value with the error at the 68% confidence level, including the estimated observational errors. Column (6) shows the dispersion of the mean value with the error at the 68% confidence level. Columns (7) and (8) show the probability to accept the hypothesis of normality, with values expressed in percentage. The normality tests show that the hypothesis of normal distribution of $|u|$ among clusters values cannot be rejected.

From Figure 4 and the average values of mean deviation presented in Table 2, we conclude that ellipticals have a mean deviation indicating more eccentric orbits than spirals. This result is of high significance and is valid both in the inner and also in the whole cluster inside the $2.5 h^{-1}$ Mpc region. A key question consists, despite of the difference in $|u|$ in Table 2, in asking if the distributions of each morphological class are originated from the same parent distribution. In particular we are interested to see if the distribution of elliptical galaxies deviations could be drawn from a population of spiral galaxies deviations. To test this hypothesis we have applied the two-sampling tests developed in IRAF/STSDAS (*twosampt* and *kolmov*), using the unbinned data. The results are summarized in Table 3, where column (1) shows the two tested populations. Column (2) and (3) show the samples defined using the same criteria as in Table 2. Column (4) shows the outer radius in h^{-1} Mpc, column (5) shows the result of the Kolmogorov-Smirnov test, the results are expressed as the probability that the two compared population came from the same parent distribution. Column (6) shows the result of the Gehan’s Generalized Wilcoxon test, again the results are expressed as the probability of both population came from the same distribution, values are given in percentage. Column (7) presents the results of Log-

rank test and column (8) the results of the Peto & Peto Generalized Wilcoxon test. The above statistical tests allow us to conclude that $|u|$ values of ellipticals and spirals indeed come from two different parent distributions, while for spirals and lenticulars they came from different population only inside the inner $1.0 h^{-1}$ Mpc region.

In Coma (402 objects) and Virgo (458 objects) we could apply a finer analysis, since these two clusters have the largest number of velocities and morphological data, in our sample. Moreover, they also deserve an special attention since they are representative of nearby clusters rich in ellipticals and spirals, respectively. In a first step we have divided the data for these two clusters into a “core” and a “halo” regions, in order to test eventual differences in these two environments. The separation radius dividing these two regions was determined by the condition of both having a similar number of objects, and not by fitting the density profile itself. So that the “core” represents the densest central region, while the “halo” the outer low density regime. The result of this analysis is presented in Table 4, divided by morphological family. We observe that in both regions remains the trend of ellipticals having lower $|u|$ than spirals. In both clusters we observe that $|u|_E \simeq 0.61$, remarkably close to the limit of radial orbit, found in our model. In contrast spirals have $|u|_S \simeq 0.80$, closer to the circular or slightly radial case.

In Figure 5 we show the radial behavior of the kurtosis, velocity dispersion and the average deviation for these two clusters and also for the MSC cluster. The continuous line refers to spirals, while the dashed line represents the ellipticals. In the Virgo cluster we used rings containing 20 object, while in Coma they contain 25 object. In the MSC as stated before the rings were defined to contain 100 objects. The velocity dispersion in the MSC cluster was scaled to 1000 km s^{-1} to ease the comparison with the corresponding plots for Virgo and Coma. We observe that the velocity dispersion has the same behavior and hence basically contains the same information as the average deviation. However, by using the average deviation we could link the orbital model and the line-of-sight velocity distribution while the same is not possible when we use the velocity dispersion. In addition, the velocity dispersion error is larger than the average deviation error, resulting therefore in a higher statistical significance. We further observe that the velocity dispersion and the average deviation profiles of MSC are

TABLE 2
AVERAGE DEVIATION IN RICH CLUSTERS

Population	sample	N	r_{outer} Mpc	$\langle u \rangle$		$\sigma_{\langle u \rangle}$	K-S %	W %
S+S0+E	All clusters	18	2.5	0.73	0.08	0.07 (-0.01,+0.02)	25	31
		18	1.0	0.73	0.08	0.07 (-0.01,+0.01)	5	50
	Without substructures	12	2.5	0.71	0.07	0.05 (-0.02,+0.01)	25	81
		12	1.0	0.71	0.07	0.06 (-0.01,+0.02)	5	7
S	All clusters	18	2.5	0.74	0.12	0.09 (-0.02,+0.01)	5	5
		18	1.0	0.80	0.17	0.10 (-0.01,+0.03)	25	15
	Without substructures	12	2.5	0.75	0.14	0.07 (-0.02,+0.02)	10	8
		12	1.0	0.81	0.17	0.08 (-0.01,+0.02)	25	33
S0	All clusters	18	2.5	0.73	0.09	0.13 (-0.02,+0.03)	25	61
		18	1.0	0.72	0.13	0.12 (-0.02,+0.03)	25	9
	Without substructures	12	2.5	0.70	0.11	0.11 (-0.03,+0.02)	25	60
		12	1.0	0.69	0.11	0.11 (-0.02,+0.03)	25	4
E	All clusters	18	2.5	0.59	0.13	0.16 (-0.02,+0.04)	25	69
		18	1.0	0.59	0.14	0.16 (-0.02,+0.04)	25	65
	Without substructures	12	2.5	0.57	0.15	0.14 (-0.04,+0.03)	25	73
		12	1.0	0.55	0.15	0.13 (-0.02,+0.04)	10	17

TABLE 3
TWO-SAMPLING TEST BETWEEN POPULATIONS

Populations	sample	N	r_{outer} Mpc	KS %	GGW %	L %	PPGW %
S x E	All clusters	18	2.5	0.2	0.1	0.02	0.7
		18	1.0	0.001	0	0	0.0001
	Without substructures	12	2.5	0.2	0.05	0	0.03
		12	1.0	0.001	0.0	0.00	0.01
S x S0	All clusters	18	2.5	27	39	20	76
		18	1.0	6	0.4	0.2	2
	Without substructures	12	2.5	10	16	3	46
		12	1.0	3	0.2	0.1	1
E x S0	All clusters	18	2.5	6	2	3	6
		18	1.0	6	2	2	6
	Without substructures	12	2.5	10	2	1	8
		12	1.0	10	2	7	10

in good agreement with the corresponding profiles of Coma and Virgo. Moreover, we can also observe that the velocity dispersion is a decreasing function of the radius, in the outer regions of all three samples.

We remark that the kurtosis profile is very noisy, even in the MSC cluster making it rather difficult to extract some useful information from this diagram.

Therefore, the tendency of ellipticals having lower $|u|$ is found in all the samples. In fact, this effect is present both in the $1.0 h^{-1}$ Mpc samples and also in the sample at $2.5 h^{-1}$ Mpc. The clusters with substructures and without substructures show the same effect and also the individual clusters as Virgo and Coma. We remark that the same effect is found in the MSC as is shown in Figures 3 and 5.

Therefore we conclude that ellipticals tend to show a systematically lower value of $|u|$, implying in more eccentric orbits, in contrast with spirals that present higher values, related with a more circular or isotropic orbit. Clusters with substructures tend to follow the same trend, although with a larger dispersion. Moreover, it is interesting to observe that lenticular galaxies tend to present an intermediate behavior between ellipticals and spirals. We remark that these trends

are also present, even if we normalize the distribution to the velocity dispersion of each morphological family instead of the velocity dispersion of all the cluster.

It is interesting compare our conclusions with the work of Biviano et al. (1992). They have compiled a sample of 68 clusters with at least 30 galaxies separating the behavior of galaxies more luminous than the third ranked galaxy (m_3). They found that the brighter galaxies are preferentially located in the central regions having in average a morphological type of $\langle T \rangle = -3$, while the less luminous ones have an average type $\langle T \rangle = -1$. They notice that this effect is not induced by morphological segregation, and is not restricted to cD clusters. Moreover it does not depend on the presence of substructures. They propose that the energy equipartition status seems to be achieved by these low velocity galaxies. Following our analysis, their Figure 2 shows a $|u|$ value of 0.55 ± 0.05 to the galaxies brighter than the third ranked galaxy and the other galaxies have a $|u|$ of 0.81 ± 0.01 . Then, a value near to circular orbits fit very well the $m > m_3$ galaxies, while for the brighter one we need more eccentric orbits.

TABLE 4
KINEMATIC PARAMETERS OF COMA AND VIRGO CLUSTERS

Sample: covered radius	population	N	v_{BI} km/s		σ_{BI} km/s		K		u	
Coma										
<i>all members</i> :0.0 - 2.0 [Mpc]	S+S0+E	458	6969	48	1032	39	0.8	0.2	0.71	0.03
	S	189	7036	79	1082	66	0.7	0.4	0.73	0.05
	S0	111	6864	106	1120	85	0.4	0.5	0.76	0.05
	E	158	6958	72	908	63	1.2	0.4	0.61	0.04
<i>core</i> :0.0 - 0.5 [Mpc]	S+S0+E	247	6918	73	1153	59	0.3	0.3	0.70	0.04
	S	94	7024	121	1172	98	-0.1	0.5	0.72	0.06
	S0	63	6877	165	1305	133	0.1	0.6	0.76	0.08
	E	90	6854	109	1030	96	0.9	0.5	0.61	0.06
<i>halo</i> :0.5 - 2.0 [Mpc]	S+S0+E	211	7036	61	894	50	1.6	0.3	0.72	0.04
	S	95	7060	103	997	85	1.8	0.5	0.78	0.07
	S0	48	6863	131	896	83	-0.6	0.7	0.80	0.05
	E	68	7084	91	748	73	0.2	0.6	0.59	0.06
Virgo										
<i>all members</i> :0.0 - 2.5 [Mpc]	S+S0+E	402	1380	39	785	23	-0.6	0.2	0.76	0.03
	S	265	1414	51	824	26	-0.8	0.3	0.82	0.03
	S0	81	1418	76	680	48	-0.6	0.5	0.65	0.05
	E	56	1172	94	701	78	0.2	0.7	0.61	0.08
<i>core</i> :0.0 - 0.8 [Mpc]	S+S0+E	213	1149	53	774	31	-0.7	0.3	0.76	0.04
	S	122	1135	76	841	44	-1.1	0.4	0.89	0.05
	S0	47	1229	91	620	72	0.0	0.7	0.55	0.07
	E	44	1082	108	706	89	0.0	0.7	0.63	0.09
<i>halo</i> :0.8 - 2.5 [Mpc]	S+S0+E	189	1629	52	710	24	-1.2	0.4	0.84	0.03
	S	143	1630	61	728	29	-1.1	0.4	0.85	0.04
	S0	34	1676	118	674	49	-1.4	0.8	0.82	0.08
	E	12	1467	194	629	135	-0.6	1.4	0.62	0.12

5. Velocity dispersion profiles

As already pointed out by other authors, in most clusters the velocity dispersion of spirals tend to be larger than the one observed in ellipticals. Actually, 13 out of the 18 clusters of the present sample show this effect.

In Figure 6 we present an histogram of the ratio of the velocity dispersions of both populations, σ_S/σ_E , sampled at two different radii. We can observe that in the internal ($< 1.0 h^{-1} \text{Mpc}$) and external regions ($< 2.5 h^{-1} \text{Mpc}$), there is a tendency for the velocity dispersion of spirals being larger. The two dotted vertical lines correspond to the median value computed on basis of the individual cluster values. Again the filled histogram correspond to the cluster without substructures. For the $1.0 h^{-1} \text{Mpc}$ region $\langle \sigma_S/\sigma_E \rangle \simeq 1.17 \pm 0.06$ with a dispersion of 0.25 ± 0.12 , while for $2.5 h^{-1} \text{Mpc}$ region we have $\langle \sigma_S/\sigma_E \rangle \simeq 1.14 \pm 0.08$ and a dispersion of 0.31 ± 0.11 . Therefore, the average velocity dispersion of spirals is $\sim 15\%$ larger than the corresponding velocity dispersion of ellipticals, but with a high variance.

From the analysis presented on section 3 we predicted that if both systems respond to the same gravitational potential their velocity dispersion would have the same value, even if the anisotropy parameter could be different. Therefore, these observed differences in velocity dispersion could imply that the initial supposition of a Gaussian distribution simply could be not true, or that both populations are not feeling the same gravitational potential. Another possibility is that this effect in the velocity dispersion could arise from differences in the dynamical state, virialized or falling models. Moreover, there might also be some contribution due to the presence of substructures inside each population.

The existence of differences in the dynamical state due to the possibility that spirals are recently falling members captured by the system and ellipticals correspond to a collapsed and virialized system, would imply in a ratio of 1.41 between the velocity dispersion of both populations. This would happen because, for spirals, the minimum energy to be bound could be expressed as $E_S = 0$, resulting that $T_S = -W_S$. On the other hand if ellipticals are virialized then $2T_E = -W_E$. Therefore, we obtain that $W_S/W_E = T_S/2T_E$, while if both systems are responding to the same potential we conclude that $T_S = 2T_E$. If both families

are affected in the same way by projection effects, having the same kind of orbits and the same spatial symmetry, we would expect that $\sigma_S = 1.41\sigma_E$. In fact, some authors (Colless & Dunn, 1996, Andreon, 1996) have used these argument favoring the idea that spirals are falling into the cluster. However, we remark from our analysis that spirals have a more isotropic rather than radial orbits. Considering the orbit information from our analysis it remains possible that spirals are in the process of capture, but in that case they are not “falling” in radial orbits into the cluster core, except perhaps for the outer ones, as can be seen in Figure 3.

An alternative explanation for the difference between the velocity dispersion of spirals and ellipticals is that they are spatially segregated inside the cluster, they could be submitted to different gravitational potentials. If we consider the density profiles ($\rho = \rho_o/r(r+b)^2$) recently discussed by Navarro et al. (1995), then we could predict that two segregated families, at radii R_E and R_S , should present virialized velocity dispersion in the ratio,

$$\frac{\sigma_S}{\sigma_E} = \left(\frac{1 - \frac{\ln(R_S/b+1)}{R_S/b}}{1 - \frac{\ln(R_E/b+1)}{R_E/b}} \right)^{1/2}$$

where b stands for the core radius of the cluster ($0.3 - 0.5 h^{-1} \text{Mpc}$). In Coma for example we would conclude, using the sample of objects with radial velocities, that the harmonic radius among spirals would be $1.01 h^{-1} \text{Mpc}$, while ellipticals have $0.83 h^{-1} \text{Mpc}$. Therefore, on basis of these estimatives we would predict $\sigma_S/\sigma_E = 1.04 - 1.05$, where the different values stands for differences in the core radius. Since for Coma $\sigma_S/\sigma_E = 1.19 \pm 0.09$, we conclude that quite probably the observed difference is not affected by this effect.

Projection effects and sub clustering could also have some influence on the observed velocity distributions. In fact, Cen (1997) using N-body simulation in a CDM universe model obtains a more quantitative estimatives of these effects. His results suggest that the presence of substructures modifies the velocity distribution in a complex way, but the final velocity dispersion is slightly affected. He estimated variations of the final velocity dispersion of only 5%, 9% and 27% within 0.5 , 1.0 and $2.0 h^{-1} \text{Mpc}$, respectively. Another study using observational data is presented in Bird et al. (1996). They noted that

the existence of substructures is an important factor to determine the dynamical parameters, but the effect is reduced when the data is restricted to a region inside the virial radius. In our case, we are working with most of the galaxies well inside of the virial radius. This supposition is respalding by the fact that r_{200} in all clusters present values always higher than the harmonic radius. Finally, it is worthwhile mention that variations on the velocity dispersion due to substructures could increase or reduce the velocity dispersions (Bird, 1994), a fact which is not consistent with spirals always presenting an slightly larger dispersion than ellipticals.

Finally, we investigate if the difference in the velocity dispersion is due to the possibility that ellipticals and spiral follow a different velocity distribution than a Gaussian. To analyze this point we referred the works of Kent & Gunn (1982), The & White (1986), Malumuth & Kriss (1986), Merritt & Saha (1993). They use different velocity and density distributions assuming different potentials, and they study the behavior of the velocity dispersion with the radius, $\sigma(r)$, instead of the total dispersion.

Kent and Gunn (1982) found that the best fit description for a rich cluster as Coma is achieved by using either an isotropic King-Michie distribution, or a constant anisotropic model. In this later case when a higher degree of anisotropy is allowed the models, for the same cluster, tend to present a lower velocity dispersions. This trend is in agreement with our findings that ellipticals have more eccentric orbits and lower velocity dispersion than spirals. In fact, from Figure 5 we can observe that in Virgo, Coma and also in the MSC we have $\sigma_E(r) < \sigma_S(r)$.

An additional constraint to the velocity distribution comes from the probable existence of a dark matter component that dominates the mass of the cluster. In this respect Merritt and Saha (1993) have investigated an interesting method to recover the gravitational potential of a cluster making use of measured line-of-sight velocity data. An application was done for the Coma cluster assuming that the potential is dominated by a dark matter halo. The first solution corresponds to a mass distribution which is slightly more concentrated than the galaxies themselves. In that case the velocity distribution is nearly radial inside $\sim 1.0 h^{-1}$ Mpc region, and isotropic outside. On the other hand two other solutions were analyze corresponding to a singular isothermal sphere, with a high density core, and an smooth halo density. In that case

the orbital distribution is isotropic inside $0.5 h^{-1}$ Mpc and circular outside. None of these three models allow for the presence of radial orbits at large radius, mainly because this solution would required a lower velocity dispersion. An alternative model to explain a velocity dispersion exceeding 600 km s^{-1} in the outer parts of Coma, was previously investigated by The & White (1986) that found equilibrium models fitting the data, assuming it as being dominated by a massive core of $\sim 10^{15} M_{\odot}$. Using these models they were able to fit the velocity dispersion data assuming that galaxies in the outer part of the cluster have nearly circular orbits.

It is worthwhile mention that although a power-law model is not a good description for Coma (Kent and Gunn, 1982), nevertheless there are clusters where this model gives a good description to the data. An example is the poor cluster MKW4 analyzed by Malumuth and Kriss (1986). In this particular case the steep dropping of the velocity dispersion profile is very well reproduced by the anisotropic power-law model. We remark however that in the present study most of our sample of rich clusters do not show such behavior and hence the constant anisotropic model, or isotropic King-Michie model, is more satisfactory.

In summary, since our sample is dominated by relatively rich clusters, the observed differences of the velocity dispersion among spirals and ellipticals is consistent with the models discussed by Kent and Gunn (1982). In this respect we favor the scenario where ellipticals have more anisotropic orbit distribution and lower dispersion. One the contrary, spirals are more representative of a population having a more isotropic, or even circular, orbit distribution and larger velocity dispersion. On possible example that illustrate these differences is the distribution of the velocity modulus for a Plummer potential shown by Merritt and Saha (1993). In fact their Monte-Carlo simulation of radial orbit models is similar distributed as the out data for ellipticals in the MSC, while their circular model have the same trend as the one we observe in spirals.

6. Conclusions

From the previous analysis we conclude that elliptical galaxies in rich regular clusters have more eccentric orbits than spirals. This effect implies that ellipticals are passing more often in the dense central regions suffering therefore a larger influence due to tidal

effects. In a first order approximation we can imagine a cluster modeled by a central mass concentration and surrounded by test particles. If we consider a typical particle having $v_R \simeq \sigma_R$ and $v_\perp \simeq \sqrt{2}\sigma_\perp$. Energy and angular momentum conservation would require that the orbit of this object should be bound to the region $R/R_G = 1 \pm \frac{\eta}{\sqrt{2+\eta^2}}$, where R_G is the cluster gravitational radius. For an isotropic orbit ($\eta = 1$) this typical object will be oscillating between $0.42 \leq R/R_G \leq 1.58$. However in the case of a typical elliptical, with $\eta \rightarrow \infty$, we have $0.0 \leq R/R_G \leq 2.00$. Therefore our average elliptical will be more exposed to the tidal interacting field of the central core objects.

The preference of ellipticals for radial orbits could be a plausible explanation why we often find two bright ellipticals in the central region of clusters. These pairs of ellipticals of comparable masses are called dumbbell galaxies (Matthews, 1964). Examples of this type of objects are NG4782/3 or the central pair in A3266 (de Souza & Quintana 1990, Quintana et al. 1996a,b). Almost 25% of the brightest cluster galaxies are multiple systems, and from a sample of 116 types BM I-II clusters extracted from the Abell catalog 51 of them have dumbbell as BCM (Gregorini et al. 1994). The ultimate evolution of a dumbbell system will be the formation a larger central object, probably a cD galaxy (Tremaine, 1990). It is interesting to observe that the presence of an spiral forming a pair in the central region of a rich cluster is a very rare event. This could be a probable consequence of the different orbital parameters of spiral and elliptical in clusters.

There are basically two scenarios that could explain the kinematical segregation found in the present work. We can imagine that clusters are generated from large amplitude perturbations. After the core formation objects in the outskirts of the cluster, preferentially spirals, are gradually accreted forming therefore an halo of objects having more circular orbits than the original objects first collapsed in the core most of them ellipticals. On the other extreme we may as well imagine a situation were large virialized groups collides given rise to a new cluster, larger than the former one, as the dynamical behavior of A2151 (Bird, 1995), or Coma (Biviano et al. 1996) in the BCG formation scenario presented by West (1994). In that case we expect that galaxies with low angular momentum will tend to cross the central regions and possibly may experience large tidal inter-

actions changing their morphologies.

We thank to the referee, E. Malumuth, for valuable comments. Also we gratefully acknowledge financial support from CAPES (AR fellowship) and FAPESP (RdS grant No 1995/7008-76). This research has made use of data obtained through the High Energy Astrophysics Science Archive Research Center Online Service, provided by the NASA/Goddard Space Flight Center.

REFERENCES

- Andernach H., 1991, ASP Conf. Ser. 15, 279
- Andreon S., 1994, A&A, 284, 801
- Andreon S., 1996, A&A, 314, 763
- Andreon S., Davoust E., 1997, A&A, 319, 747
- Beers T.C., Flynn K., Gebhardt K., 1990, AJ, 100, 32
- Bird C.M., 1994, AJ, 107, 1637
- Bird C.M., 1995, ApJ, 445, L81
- Bird C.M., Davis D.S., Beers T.C., 1994, AJ, 109, 920
- Biviano A., Girardi M., Giuricin G., Mardirossian F., Mezetti M., 1992, ApJ, 396, 35
- Biviano A., Durret F., Gerbal D., Le Fèvre O., Lobo C., Mazure A., Slezak E., 1996, A&A, 311, 95
- Biviano A., Katgert P., Mazure A., Moles M., den Hartog R., Perea J., Focardi P., 1997, A&A, 321, 84
- Bower R., 1995 in *Dahlem Workshop Proceeding "The Evolution of the Universe"*. astro-ph/9511058
- Carlberg R.G., Yee H.K.C., and Ellingson E., 1997, ApJ, 478, 462
- Cen R., 1997, ApJ, 485, 39
- Colless M., Dunn A.M., 1996, ApJ, 458, 435
- de Souza R., Quintana H., 1990, AJ99, 1065
- de Vaucouleurs G., de Vaucouleurs A., Corwin H.G.Jr., Buta R.J., Fouque P., Paturel G., 1991, *The Third Reference Catalogue of Bright Galaxies (RC3)*, by Springer-Verlag, New York.

- Dressler A., 1980a, ApJ, 236, 351
- Dressler A., 1980b, ApJS, 42, 565
- Dressler A., Shectman S.A., 1988, AJ, 95, 985
- Fabricant D., Kurtz M., Geller M., Zabludoff A., Mack P., Wegner G., 1993, AJ105, 788
- Fadda D., Girardi M., Giuricin G., Mardirossian F., Mezetti M., 1996, ApJ, 473, 670
- Ferguson H.C., 1989, AJ98, 367
- Girardi M., Fadda D., Giuricin G., Mardirossian F., Mezetti M., 1996, ApJ457, 61
- Gregorini L., Vettolani G., de Ruiter H.R., Parma P., 1992, A&AS, 95, 1
- Huchra J.P., 1985, *The Virgo Cluster*, ESO Workshop Proceedings N° 20, eds. Richter O.-G., Binggeli B., (Munich: ESO), p. 181
- Huchra J.P., Geller M.J., Clemens C.M., Tokarz S.P., Michel A., 1992 *The CfA Redshift Catalogue* Harvard-Smithsonian Center for Astrophysics, Cambridge, MA
- Katz N., White S.D.M., 1993, ApJ, 412, 455
- Kendall M., Stuart A., Ord J.K., 1987 *Kendall's Advanced Theory of Statistics*, fifth edition of Volume 1: Distribution Theory, p.52 (Charles Griffin & Co.Ltd., London).
- Malumuth E.M., Kriss G.A., 1986, ApJ, 308, 10
- Malumuth E.M., Kriss G.A., Van Dyke Dixon W., Ferguson H.C., Ritchie C., 1992, AJ104, 495
- Matthews T.A., Morgan W.W., Schmidt M., 1964, ApJ140, 35
- Merritt D., 1988, in *The Minnesota Lectures on Clusters of Galaxies and Large-Scale Structure*, Astron. Soc. of the Pacific Conf. Ser. Vol.5, Ed. by J.M. Dickey (Brigham Young University Print Service, Provo), p. 175
- Merritt D., Gebhardt K. 1995, in *Rencontres de Moriond, "Cluster of Galaxies"*, ed. by F. Durret (astro-ph/9510091)
- Merritt D., Saha P., 1993, ApJ, 409, 75
- Moss C., Dickens R.J., 1977, MNRAS, 178, 701
- Navarro J.F., Frenk C.S., White S.D.M., 1995, MNRAS, 275, 56
- Paturel G., Fouque P., Bottinelli L., Gougenheim L., 1989, A&AS, 80, 299
- Quintana H., Ramírez A., Way M.J., 1996, AJ, 111, 603
- Quintana H., Ramírez A., Way M.J., 1996, AJ, 112, 36
- Roettinger K., Burns J.O., Loken C., 1993, ApJ, 407, L53
- Saslaw W.C., Chitre S.M., Itoh M., Inagaki S., 1990, ApJ, 365, 419
- Scodreggio M., Solanes J.M., Giovanelli R., Haynes M., 1995, ApJ, 444, 41
- Sodré L., Capelato H., Steiner J., 1989, AJ, 97, 1279
- The L.S., White S.D.M., 1986, AJ, 96, 1248
- Tremaine S., 1990, in *Dynamics and Interactions of Galaxies*, ed. by R. Wielen (Springer, Berlin) p. 394
- Tully R.B., Shaya E.J. 1984, ApJ, 281, 31
- Ueda H., Itoh M., Suto Y., 1993, ApJ, 408, 3
- Valentijn E.A., Casertano S., 1988, A&A, 20, 27
- Whitmore B.C., Gilmore D.M., 1991, ApJ, 367, 64
- Wirth A., Smarr L., Gallagher J.J., 1982, AJ, 87, 602
- Yahil A., Vidal N., 1977, ApJ, 214, 347
- Zabludoff A.I., Franx M., Geller M.J., 1993, ApJ, 419, 47

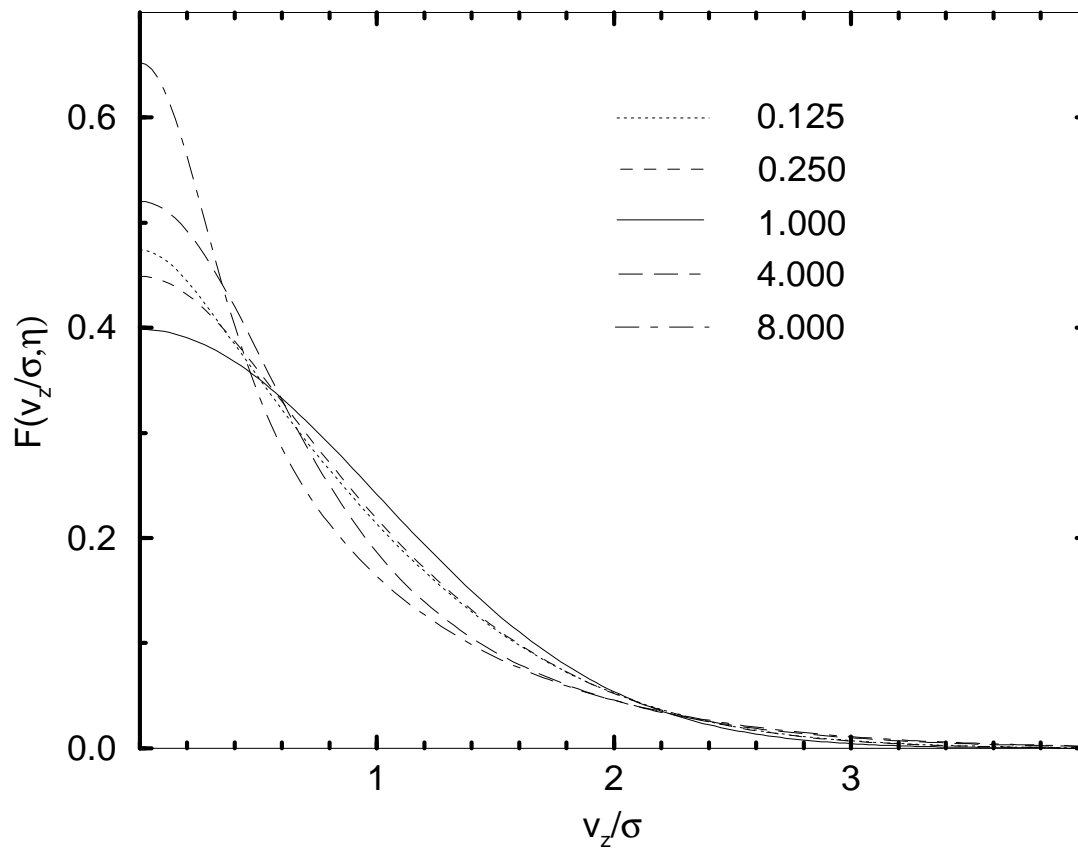


Fig. 1.— Velocity distribution along the line-of-sight normalized to the velocity dispersion for different values of the anisotropic parameter. The smallest central peak value, and also the kurtosis, corresponds to the case of an isotropic distribution (continuous line), that results in a Gaussian curve.

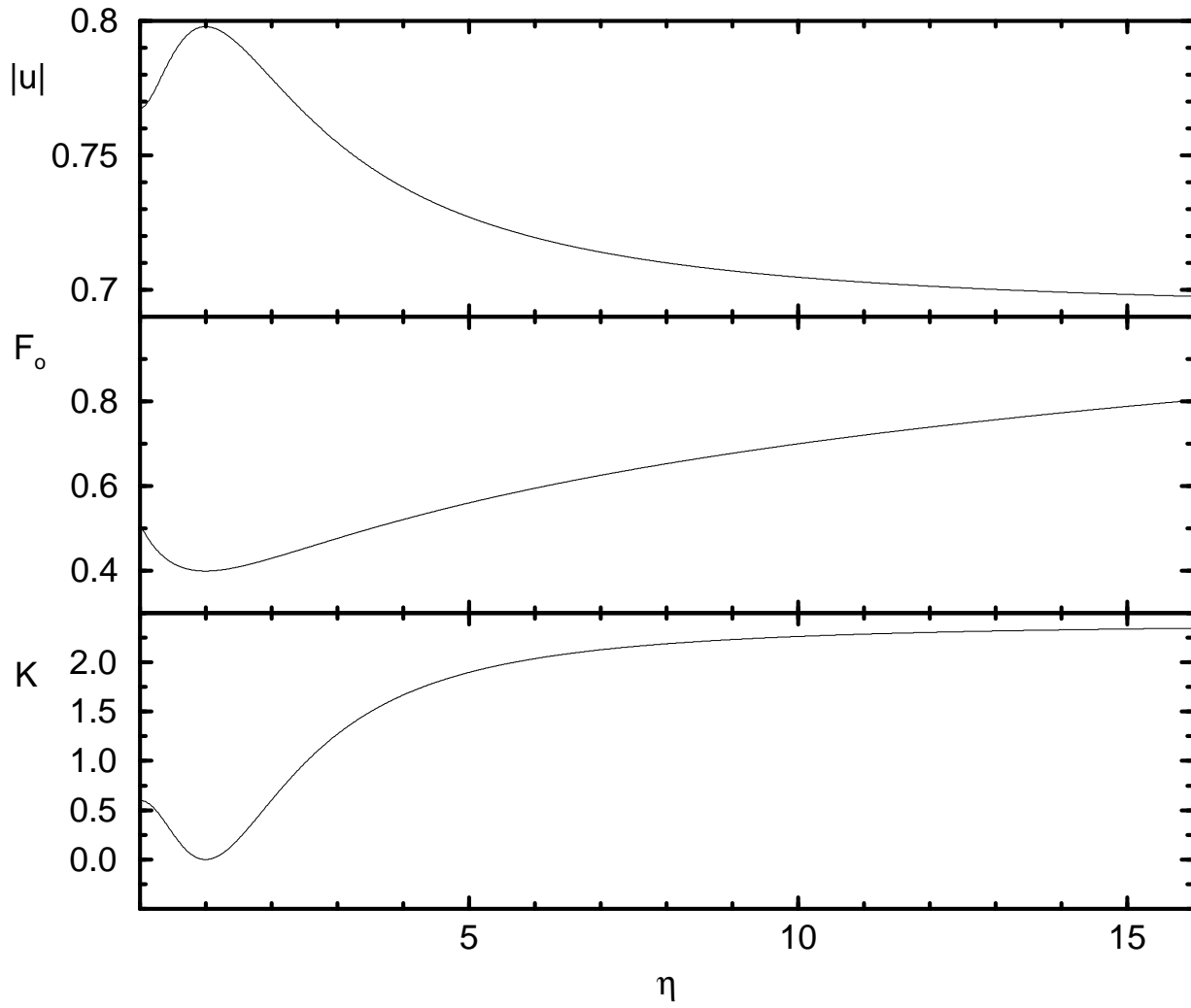


Fig. 2.— Behavior of kurtosis, central peak value and mean velocity modulus for a family of distribution functions, having the same velocity dispersion but different values of the anisotropy parameter values.

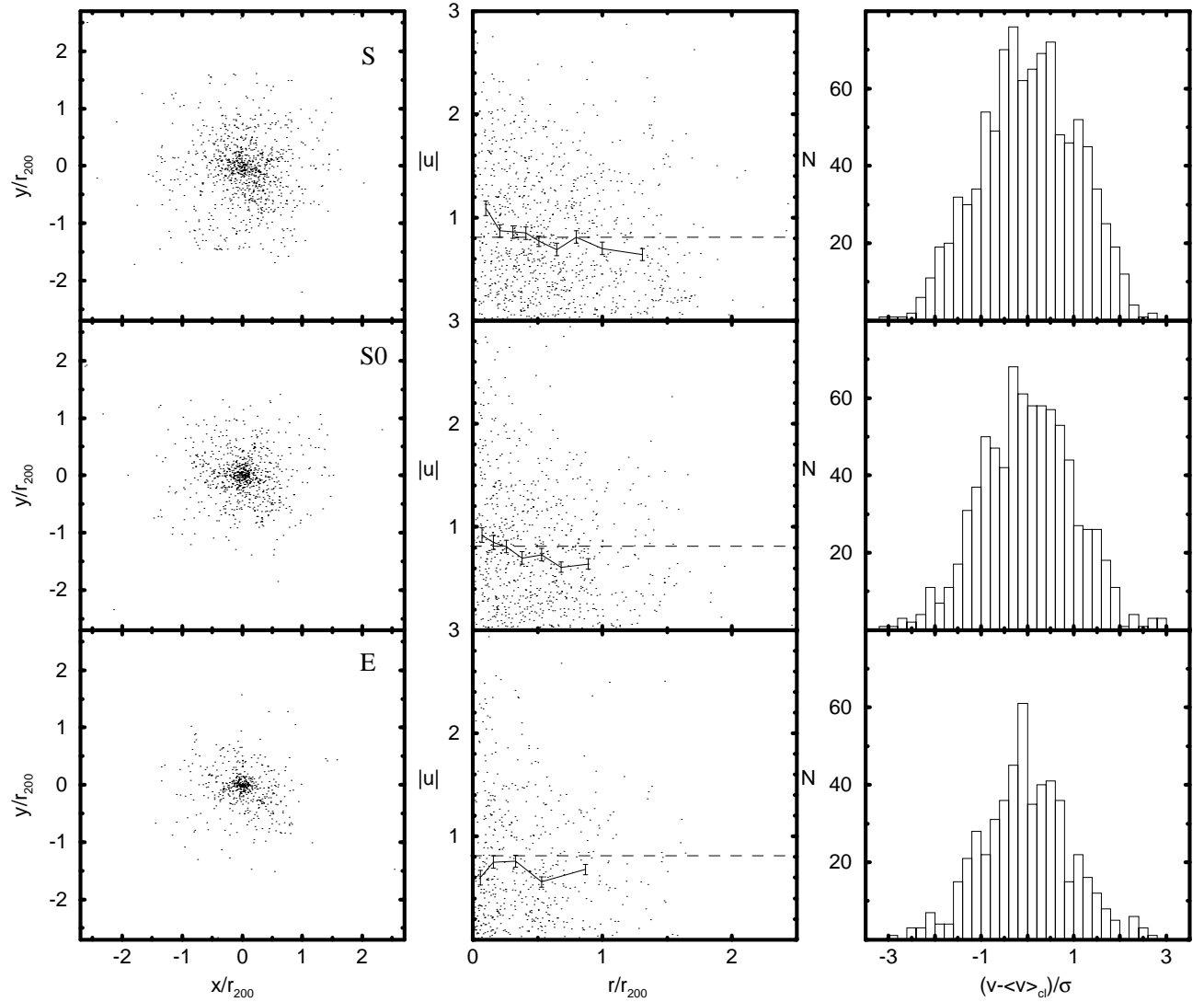


Fig. 3.— Mean Synthetic cluster (MSC) for spiral (top), lenticular (middle) and elliptical (bottom). In the left panels the projected positions are in units of r_{200} . In the middle panels it is presented the modulus of the velocity normalized to the velocity dispersion. The solid lines correspond to the average deviation within rings of 100 galaxies each, and the error bars are at the 68% confidence level. Right panels: histograms of the velocities relative to the mean cluster velocity normalized to the projected velocity dispersion of the corresponding cluster, bins are 200 km/s width.

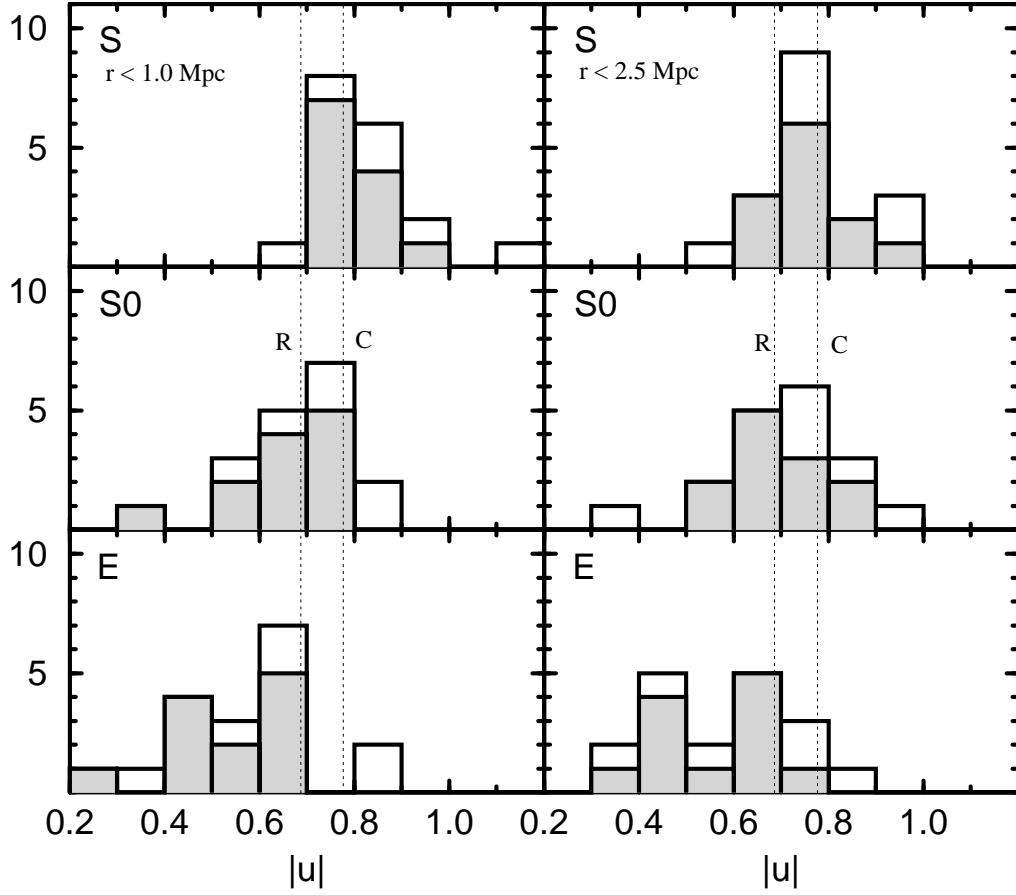


Fig. 4.— The cluster sample distribution of the average deviation of the line-of-sight velocity. Histograms of the spiral, lenticular and elliptical populations inside $1.0 h^{-1}$ Mpc and $2.5 h^{-1}$ Mpc are plotted at right and left side, respectively. The filled histograms represent clusters without significant substructures, the open histograms show the contribution of clusters where there might be some suspicious substructures as detected by Girardi et al. (1996). The vertical dashed lines show the expected value for the extreme cases of radial (R) and circular (C) orbits.

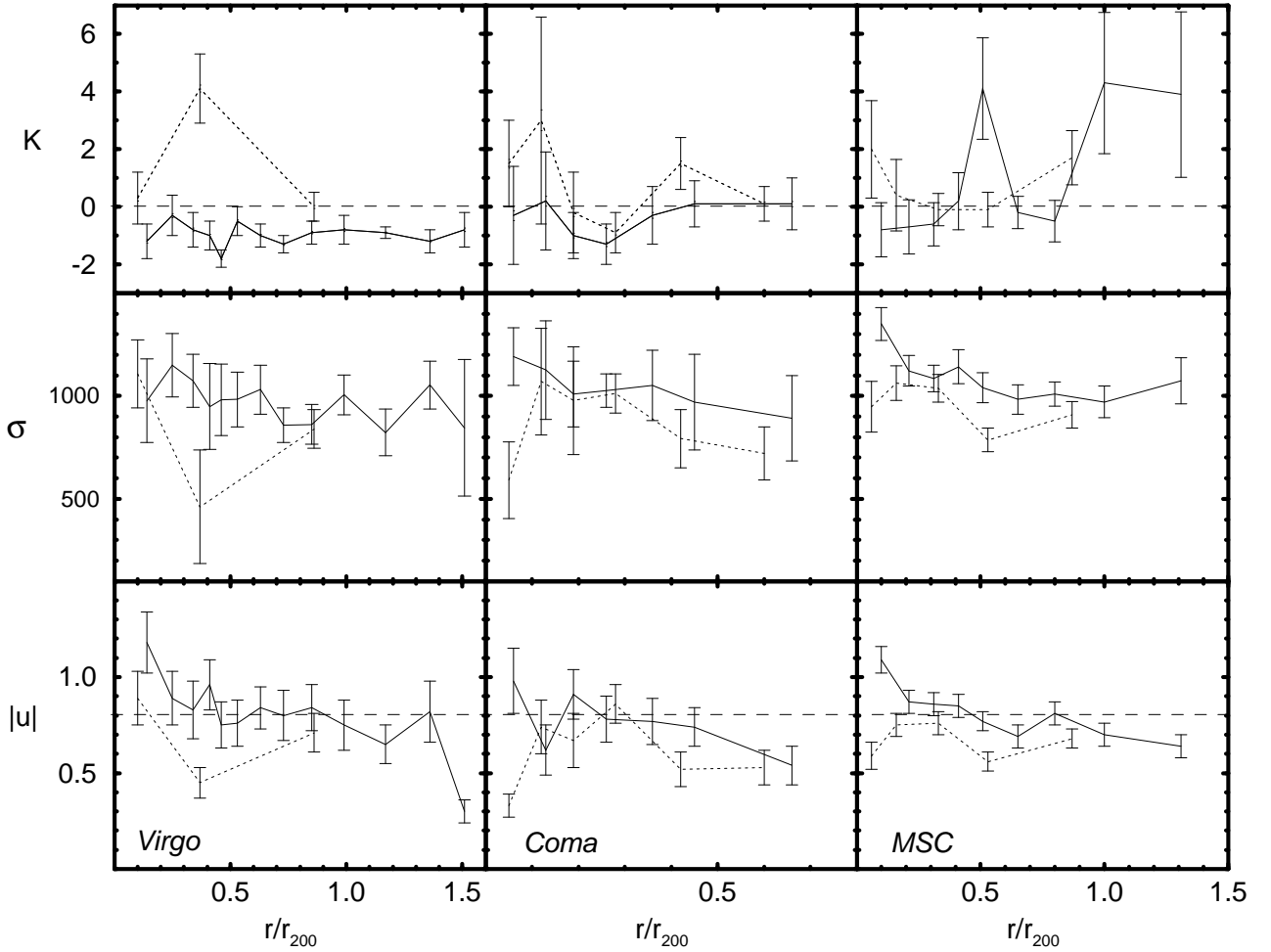


Fig. 5.— The kurtosis, velocity dispersion and average deviation as a function of the radius for Virgo, Coma and the MSC clusters. The radius is expressed in unit of r_{200} . Estimatives of these parameters were done using rings with 20, 25 and 100 galaxies, in Virgo, Coma and MSC respectively. Solid lines represent the spirals and dotted lines the ellipticals. Error bars are at the 68% confidence level. The long dashed line presented in the kurtosis and average deviation plots correspond to the expectation value when orbits are isotropic

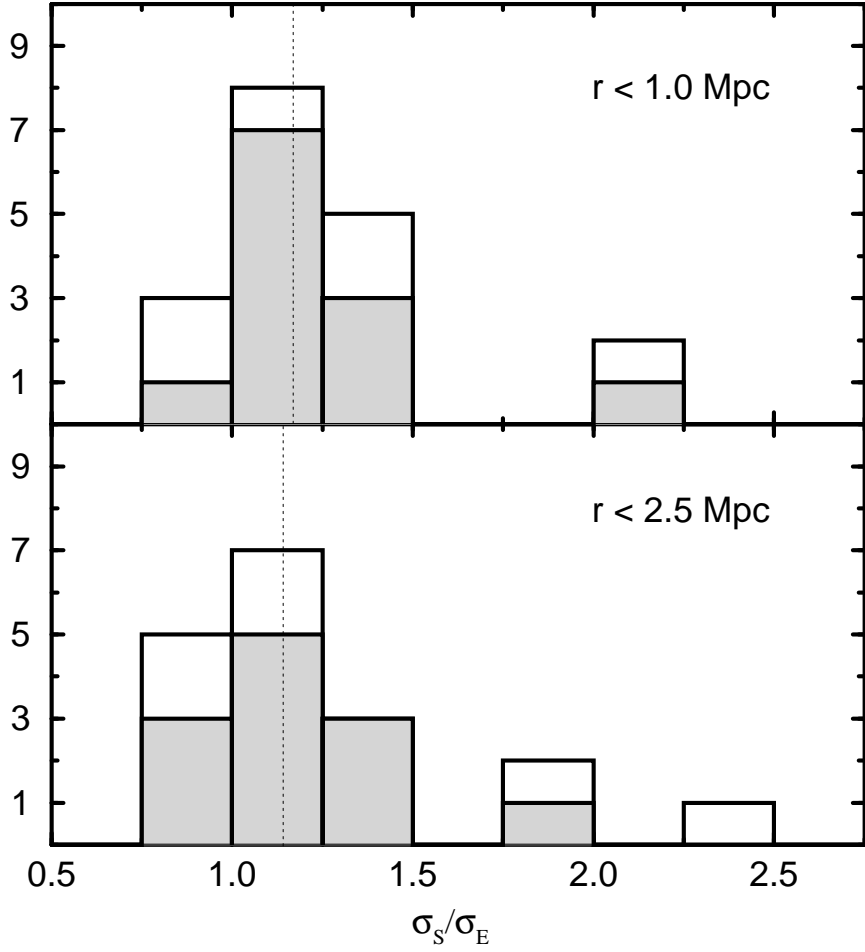


Fig. 6.— Histogram of the ratio of velocity dispersions between spirals and ellipticals in 18 nearby clusters. Upper plots show the distribution considering all members inside $1.0 h^{-1}$ Mpc , while the data for $2.5 h^{-1}$ Mpc is in the lower panels. The two vertical lines correspond to the median values.

TABLE 1

CLUSTER KINEMATIC PARAMETERS USING THE ELLIPTICAL, SPIRAL AND LENTICULAR GALAXIES

Name	N	r_{200} Mpc	r_h Mpc	v_{BI} km/s	σ_{BI} km/s	K	$ u _{cl}$	$\sigma_{ u }$	References					
All														
A1656	458	1.8	0.9	6969	48	1032	39	0.8	0.22	0.71	0.03	0.59	0.03	zcat; CD95 ^a &B96 ^b
Virgo	402	1.4	1.4	1380	39	785	23	-0.6	0.24	0.76	0.03	0.55	0.02	zcat
A3526	287	1.5	1.2	3436	51	863	34	-0.7	0.29	0.75	0.04	0.60	0.02	zcat; Centaurus
A0194	146	0.7	0.9	5338	33	398	28	1.1	0.41	0.71	0.05	0.64	0.06	zcat
A0548	128	1.5	1.4	12407	77	870	45	-0.9	0.43	0.83	0.05	0.52	0.03	zcat
A1060	98	1.1	0.7	3668	64	631	44	-0.5	0.49	0.74	0.06	0.59	0.04	zcat; Hydra
A2151	93	1.3	1.3	11000	76	735	46	-0.7	0.51	0.80	0.06	0.59	0.04	zcat; Hercules
A1644	89	1.6	1.6	14129	99	934	84	0.3	0.52	0.67	0.06	0.59	0.09	zcat
A0539	83	1.2	0.8	8721	79	715	72	0.2	0.54	0.66	0.07	0.67	0.07	zcat
A463s	79	1.1	1.1	12275	71	624	37	-0.9	0.55	0.83	0.06	0.51	0.04	zcat; DC0428-53
A0496	77	1.1	0.6	9836	71	620	67	0.4	0.56	0.64	0.08	0.66	0.09	zcat
	138			9870	62	728	49	0.0	0.42	0.70	0.05			M92 ^c
A3376	77	1.3	1.1	13909	84	737	72	0.3	0.56	0.70	0.08	0.65	0.07	zcat; DC0559-40
A805s	77	0.7	0.7	4351	48	419	38	0.1	0.56	0.71	0.07	0.57	0.06	zcat; DC1842-63
	114			4513	47	503	44	0.1	0.46	0.66	0.06			M92 ^c
A0119	76	1.5	0.9	13324	97	840	91	0.0	0.56	0.66	0.08	0.68	0.08	F93 ^d
A0754	72	1.4	1.4	16257	96	812	84	-0.1	0.58	0.70	0.08	0.64	0.08	zcat
A1983	72	1.1	1.5	13562	78	660	153	1.5	0.58	0.52	0.07	0.56	0.10	zcat
A1631	68	1.2	1.5	13971	85	696	50	-0.6	0.59	0.79	0.07	0.58	0.04	zcat
Fornax	66	0.6	0.7	1483	41	330	24	-0.6	0.60	0.76	0.07	0.58	0.05	F89 ^e
Spirals														
A1656	189	1.9	1.0	7036	79	1082	66	0.7	0.36	0.73	0.05	0.61	0.04	
Virgo	265	1.4	1.6	1414	51	824	26	-0.8	0.30	0.82	0.03	0.57	0.02	
A3526	155	1.5	1.7	3390	67	838	51	0.6	0.39	0.71	0.05	0.59	0.04	
A0194	76	0.7	1.4	5306	47	410	32	-0.2	0.56	0.78	0.06	0.63	0.11	
A0548	45	1.7	1.4	12407	151	1002	81	-1.1	0.73	0.97	0.09	0.59	0.05	
A1060	36	1.1	1.1	3506	103	611	50	-0.6	0.82	0.72	0.10	0.57	0.08	
A2151	45	1.2	1.1	11265	106	706	64	-0.4	0.73	0.72	0.09	0.65	0.05	
A1644	23	1.7	1.8	13808	211	987	171	-0.1	1.02	0.68	0.13	0.69	0.11	
A0539	41	1.0	1.6	8726	94	597	85	0.1	0.77	0.53	0.08	0.50	0.09	
A463s	18	1.3	1.7	12215	186	754	114	-1.0	1.15	0.95	0.17	0.67	0.10	
A0496	18	1.1	1.2	10055	150	612	102	-0.8	1.15	0.74	0.13	0.63	0.15	
A3376	24	1.3	1.3	13845	164	779	122	-0.1	1.00	0.75	0.13	0.60	0.12	
A805s	39	0.8	1.7	4395	70	434	63	0.0	0.78	0.70	0.11	0.65	0.10	
A0119	15	1.7	1.3	13687	261	959	143	-1.0	1.26	0.94	0.17	0.68	0.10	
A0754	25	1.5	1.6	16347	178	869	156	-0.2	0.98	0.75	0.14	0.71	0.19	
A1983	31	2.1	1.5	13353	220	1194	426	0.3	0.88	0.72	0.23	1.10	0.63	
A1631	16	1.2	1.5	14215	178	676	139	0.0	1.22	0.70	0.14	0.62	0.10	
Fornax	22	0.6	0.8	1548	82	371	52	-0.9	1.04	0.84	0.13	0.56	0.07	
Lenticulars														
A1656	111	1.9	0.8	6864	106	1120	85	0.4	0.46	0.76	0.05	0.58	0.06	
Virgo	81	1.2	1.0	1418	76	680	48	-0.6	0.54	0.65	0.05	0.46	0.05	
A3526	85	1.5	1.1	3501	96	878	77	-0.6	0.53	0.72	0.07	0.65	0.04	
A0194	35	0.6	0.7	5397	57	330	89	-0.8	0.83	0.53	0.10	0.54	0.13	
A0548	52	1.4	1.3	12415	110	784	57	-1.0	0.68	0.75	0.07	0.50	0.03	
A1060	49	1.1	0.6	3795	93	642	52	-0.8	0.70	0.79	0.08	0.60	0.05	
A2151	36	1.3	1.2	10855	130	768	64	-1.2	0.82	0.89	0.08	0.56	0.07	
A1644	47	1.5	1.5	14207	124	840	104	0.5	0.71	0.64	0.08	0.48	0.09	
A0539	31	1.6	0.5	8726	167	911	126	-0.9	0.88	0.94	0.15	0.82	0.09	
A463s	39	1.0	1.2	12238	96	592	57	-0.5	0.78	0.78	0.09	0.52	0.05	
A0496	32	1.3	0.5	9706	132	733	108	-0.1	0.87	0.85	0.14	0.80	0.12	
A3376	40	1.4	1.2	13846	128	801	104	0.2	0.77	0.79	0.11	0.71	0.10	
A805s	29	0.6	0.6	4351	70	368	39	2.2	0.91	0.69	0.09	0.46	0.06	
A0119	36	1.3	1.1	13243	123	729	121	0.5	0.82	0.55	0.08	0.56	0.11	
A0754	25	1.2	1.5	16072	140	680	82	-0.9	0.98	0.67	0.11	0.50	0.06	
A1983	27	0.7	1.7	13681	83	422	286	1.0	0.94	0.37	0.08	0.35	0.13	
A1631	43	1.3	1.4	13941	112	728	71	-0.6	0.75	0.82	0.09	0.60	0.06	
Fornax	24	0.6	0.6	1507	68	323	49	-0.2	1.00	0.68	0.10	0.51	0.10	
Ellipticals														
A1656	158	1.6	0.8	6958	72	908	63	1.2	0.39	0.61	0.04	0.55	0.05	
Virgo	56	1.2	0.8	1172	94	701	78	0.2	0.65	0.61	0.08	0.50	0.06	
A3526	47	1.6	0.7	3472	133	902	66	-1.2	0.71	0.86	0.08	0.54	0.04	
A0194	35	0.7	0.9	5344	68	398	66	1.5	0.83	0.64	0.11	0.65	0.12	
A0548	31	1.5	1.3	12391	154	841	93	-0.7	0.88	0.78	0.08	0.45	0.07	
A1060	13	1.0	0.6	3660	175	596	166	0.0	1.36	0.48	0.16	0.49	0.40	

TABLE 1—*Continued*

Name	N	r_{200} Mpc	r_h Mpc	v_{BI} km/s	σ_{BI} km/s	K		$ u _{cl}$		$\sigma_{ u }$		References	
A2151	12	0.6	1.6	10522	114	369	53	-1.4	1.41	0.44	0.08	0.47	0.06
A1644	19	1.8	1.9	14252	254	1067	244	-0.3	1.12	0.70	0.18	0.75	0.25
A0539	11	1.0	0.2	8729	194	601	279	0.4	1.48	0.38	0.19	0.56	0.37
A463s	22	1.1	1.0	12495	143	649	209	-1.3	1.04	0.75	0.13	0.32	0.05
A0496	27	0.8	0.2	9818	88	445	126	1.5	0.94	0.43	0.09	0.46	0.09
A3376	13	0.7	0.5	14050	123	417	133	0.4	1.36	0.33	0.05	0.39	0.22
A805s	9	0.9	0.3	4111	186	507	151	-0.4	1.63	0.70	0.19	0.81	0.30
A0119	24	1.5	0.6	13394	180	859	349	-0.1	1.00	0.42	0.14	0.79	0.42
A0754	22	1.5	0.8	16451	195	885	167	-0.2	1.04	0.77	0.16	0.76	0.24
A1983	14	0.9	0.6	13575	145	514	111	-0.9	1.31	0.57	0.12	0.42	0.11
A1631	9	0.9	0.9	13706	181	493	85	-1.4	1.63	0.60	0.13	0.46	0.14
Fornax	20	0.5	0.5	1396	64	277	80	-0.1	1.10	0.49	0.14	0.58	0.60

^aColless and Dunn (1996)

^bBiviano et al.(1996)

^cMalumuth et al. (1992)

^dFabricant et al. (1993)

^eFerguson (1989)

TABLE 2
AVERAGE DEVIATION IN RICH CLUSTERS

Population	sample	N	r_{outer} Mpc	$\langle u \rangle$		$\sigma_{\langle u \rangle}$	K-S %	W %
S+S0+E	All clusters	18	2.5	0.73	0.08	0.07 (-0.01,+0.02)	25	31
		18	1.0	0.73	0.08	0.07 (-0.01,+0.01)	5	50
	Without substructures	12	2.5	0.71	0.07	0.05 (-0.02,+0.01)	25	81
		12	1.0	0.71	0.07	0.06 (-0.01,+0.02)	5	7
S	All clusters	18	2.5	0.74	0.12	0.09 (-0.02,+0.01)	5	5
		18	1.0	0.80	0.17	0.10 (-0.01,+0.03)	25	15
	Without substructures	12	2.5	0.75	0.14	0.07 (-0.02,+0.02)	10	8
		12	1.0	0.81	0.17	0.08 (-0.01,+0.02)	25	33
S0	All clusters	18	2.5	0.73	0.09	0.13 (-0.02,+0.03)	25	61
		18	1.0	0.72	0.13	0.12 (-0.02,+0.03)	25	9
	Without substructures	12	2.5	0.70	0.11	0.11 (-0.03,+0.02)	25	60
		12	1.0	0.69	0.11	0.11 (-0.02,+0.03)	25	4
E	All clusters	18	2.5	0.59	0.13	0.16 (-0.02,+0.04)	25	69
		18	1.0	0.59	0.14	0.16 (-0.02,+0.04)	25	65
	Without substructures	12	2.5	0.57	0.15	0.14 (-0.04,+0.03)	25	73
		12	1.0	0.55	0.15	0.13 (-0.02,+0.04)	10	17

TABLE 3
TWO-SAMPLING TEST BETWEEN POPULATIONS

Populations	sample	N	r_{outer} Mpc	KS %	GGW %	L %	PPGW %
S x E	All clusters	18	2.5	0.2	0.1	0.02	0.7
		18	1.0	0.001	0	0	0.0001
	Without substructures	12	2.5	0.2	0.05	0	0.03
		12	1.0	0.001	0.0	0.00	0.01
S x S0	All clusters	18	2.5	27	39	20	76
		18	1.0	6	0.4	0.2	2
	Without substructures	12	2.5	10	16	3	46
		12	1.0	3	0.2	0.1	1
E x S0	All clusters	18	2.5	6	2	3	6
		18	1.0	6	2	2	6
	Without substructures	12	2.5	10	2	1	8
		12	1.0	10	2	7	10

TABLE 4
KINEMATIC PARAMETERS OF COMA AND VIRGO CLUSTERS

Sample: covered radius	population	N	v_{BI} km/s		σ_{BI} km/s		K		u	
Coma										
<i>all members</i> :0.0 - 2.0 [Mpc]	S+S0+E	458	6969	48	1032	39	0.8	0.2	0.71	0.03
	S	189	7036	79	1082	66	0.7	0.4	0.73	0.05
	S0	111	6864	106	1120	85	0.4	0.5	0.76	0.05
	E	158	6958	72	908	63	1.2	0.4	0.61	0.04
<i>core</i> :0.0 - 0.5 [Mpc]	S+S0+E	247	6918	73	1153	59	0.3	0.3	0.70	0.04
	S	94	7024	121	1172	98	-0.1	0.5	0.72	0.06
	S0	63	6877	165	1305	133	0.1	0.6	0.76	0.08
	E	90	6854	109	1030	96	0.9	0.5	0.61	0.06
<i>halo</i> :0.5 - 2.0 [Mpc]	S+S0+E	211	7036	61	894	50	1.6	0.3	0.72	0.04
	S	95	7060	103	997	85	1.8	0.5	0.78	0.07
	S0	48	6863	131	896	83	-0.6	0.7	0.80	0.05
	E	68	7084	91	748	73	0.2	0.6	0.59	0.06
Virgo										
<i>all members</i> :0.0 - 2.5 [Mpc]	S+S0+E	402	1380	39	785	23	-0.6	0.2	0.76	0.03
	S	265	1414	51	824	26	-0.8	0.3	0.82	0.03
	S0	81	1418	76	680	48	-0.6	0.5	0.65	0.05
	E	56	1172	94	701	78	0.2	0.7	0.61	0.08
<i>core</i> :0.0 - 0.8 [Mpc]	S+S0+E	213	1149	53	774	31	-0.7	0.3	0.76	0.04
	S	122	1135	76	841	44	-1.1	0.4	0.89	0.05
	S0	47	1229	91	620	72	0.0	0.7	0.55	0.07
	E	44	1082	108	706	89	0.0	0.7	0.63	0.09
<i>halo</i> :0.8 - 2.5 [Mpc]	S+S0+E	189	1629	52	710	24	-1.2	0.4	0.84	0.03
	S	143	1630	61	728	29	-1.1	0.4	0.85	0.04
	S0	34	1676	118	674	49	-1.4	0.8	0.82	0.08
	E	12	1467	194	629	135	-0.6	1.4	0.62	0.12